materials

MDPI

Article

Selective Laser Spectroscopy of the Bixbyite-Type Yttrium Scandate Doped by Rare-Earth Ions

Elena Dobretsova *, Olimkhon Alimov, Sergey Rusanov, Vitaly Kashin and Vladimir Tsvetkov

Prokhorov General Physics Institute of the Russian Academy of Sciences, 119991 Moscow, Russia; olim@lst.gpi.ru (O.A.); rusanov@lsk.gpi.ru (S.R.); kashin@lsk.gpi.ru (V.K.); tsvetkov@lsk.gpi.ru (V.T.)
* Correspondence: elenadobretsova89@gmail.com or eadobr@kapella.gpi.ru

Abstract: Yttrium scandate crystals doped by Nd^{3+} and Tm^{3+} ions have been successfully grown in the form of fibers using the laser-heated pedestal growth (LHPG) technique. The selective laser spectroscopy methods have identified and distinguished three distinct types of optically active centers associated with Nd^{3+} and Tm^{3+} ions. The substitution of Y^{3+} and Sc^{3+} for rare-earth ions in the C_2 structural site leads to the formation of two distinct basic long-time centers. In Nd^{3+}:$YScO_3$, another type of center (a short-lifetime one) is formed known as the Nd^{3+}–Nd^{3+} aggregate pair. This center arises from the substitution of Y^{3+} or Sc^{3+} for Nd^{3+} cation in the adjacent MO_6 polyhedra that share an edge. In Tm^{3+}:$YScO_3$, the third optical center is formed as a result of the substitution of Y^{3+} or Sc^{3+} for Tm^{3+} in the MO_6 octahedra with the C_{3i} site symmetry. The fluorescence decay lifetimes of Nd^{3+} and Tm^{3+} ions in the $YScO_3$ crystal structure have been accurately measured and estimated. A Stark level diagram illustrating the splitting of $^4F_{3/2}$, $^4I_{11/2}$, and $^4I_{9/2}$ multiplets of Nd^{3+} ions has been constructed to show features of the active optical centers with the C_2 site symmetry.

Keywords: selective laser spectroscopy; optical center; rare-earth ion

check for updates

Citation: Dobretsova, E.; Alimov, O.; Rusanov, S.; Kashin, V.; Tsvetkov, V. Selective Laser Spectroscopy of the Bixbyite-Type Yttrium Scandate Doped by Rare-Earth Ions. *Materials* **2023**, *16*, 6829. https://doi.org/10.3390/ma16216829

Academic Editor: Valery V. Tuchin

Received: 8 September 2023
Revised: 20 October 2023
Accepted: 21 October 2023
Published: 24 October 2023

Copyright: © 2023 by the authors. Licensee MDPI, Basel, Switzerland. This article is an open access article distributed under the terms and conditions of the Creative Commons Attribution (CC BY) license (https://creativecommons.org/licenses/by/4.0/).

1. Introduction

Rare-earth (RE^{3+})-doped Sc_2O_3 and Y_2O_3 sesquioxides exhibit high thermal conductivity, approximately twice that of yttrium aluminum (YAG) [1], and have a wide transparency range from 0.25 μm to 9.6 μm [2]. These materials have demonstrated excellent potential for high-power solid-state lasers [3–8], particularly in the infrared (IR) spectral region. They could serve as a viable alternative to the well-established YAG crystals. RE^{3+}-doped sesquioxide materials show strong potential for a variety of applications, including solid-state light-emitting devices [9–11], high-efficiency luminescent materials [12,13], rare-earth magnets [14,15], magneto-optical recording materials [16,17], and so on.

Both Y_2O_3 and Sc_2O_3 are categorized as a cubic bixbyite-type structure [18–22], where there are one position for the oxygen ion and two symmetrically independent positions for cations: the 8*b* site with C_{3i} symmetry and 24*d* site with C_2 symmetry. The unit cell contains three cations occupying the the C_2 site and one cation in the C_{3i} site. Two types of 6-vertex polyhedra share corners and edges to form a chessboard packing derived from the fluorite structure type [23].

Extensive research has been carried out on rare-earth dopants in Y_2O_3 crystals, revealing that RE^{3+} ions have the capability to occupy Y^{3+} sites [24–31]. However, due to inversion symmetry, the electric dipole–dipole transitions within the 4*f*-configuration are forbidden for the Kramers RE^{3+} ions (which have an odd number of 4*f*-electrons) occupying the C_{3i} sites. Consequently, all electron transitions observed in the fluorescence spectra of these ions should be assigned to electronic transitions in active optical centers located in the C_2 sites. Sc_2O_3 is also a promising host material as it exhibits a strong crystal field effect, primarily caused by the lattice distortions resulting from the substitution of Sc^{3+} for RE^{3+} ions of larger size [4,32,33]. Moreover, Tm^{3+}-doped Sc_2O_3 and Y_2O_3 have extraordinary

broad gain spectra around 2 μm. In comparison to YAG, the peak emission cross-section of the Tm^{3+} ion at 2 μm is four times greater in both Sc_2O_3 and Y_2O_3 [32].

Yttrium scandate ($YScO_3$) has a polymorphic nature, implying that the laser properties can be varied depending on the host crystal structure and the type of rare-earth ions. Additionally, mixed sesquioxides demonstrate notably lower melting temperatures compared to yttria and scandia. Mixed sesquioxides hold great promise for the generation and amplification of ultrashort pulses [6,34,35]. This is due to their inhomogeneously broadened gain spectra, which is a result of the intrinsic disorder in the crystal structure [35]. Nd lasers have been realized successfully in the $YScO_3$ and isostructural $(Lu_{1-x}Sc_x)_2O_3$ mixed seqioxides [36]. The high-temperature modification of $YscO_3$ belongs to the bixbyite-type structure [18,20,37,38] similar to yttria (Y_2O_3) [21] and scandia (Sc_2O_3) [22]. It can be "frozen" during the crystal growth process, and the synthesis method used plays a critical role. The features of the laser-heated pedestal growth (LHPG) technique are high temperature of heating under laser irradiation followed by rapid cooling. The method allows one to obtain crystals in the form of fibers [39,40].

There is a high probability that certain rare-earth optical centers will be formed in the disordered structure. Selective laser spectroscopy methods are particularly suitable for studying optical properties of rare-earth-doped laser active media such as yttrium scandate.

We have conducted a comprehensive spectral–kinetic analysis of both Nd^{3+}:$YScO_3$ and Tm^{3+}:$YScO_3$ crystal fibers using the methods of selective laser spectroscopy.

2. Materials and Methods

Crystals of 0.1 at. % Nd^{3+}:$YScO_3$ and 0.1 at. % Tm^{3+}:$YScO_3$ have been obtained using the laser-heated pedestal growth (LHPG) technique. Commercial powders of Y_2O_3 and Sc_2O_3 (purity > 99.999%, Sigma Aldrich, Burlington, MA, USA) were used as precursors, while Nd_2O_3 and Tm_2O_3 powders (purity > 99.999%, Sigma Aldrich, Burlington, MA, USA) were used as activators. Both Nd^{3+}:$YScO_3$ and Tm^{3+}:$YScO_3$ crystals have been grown in the form of fibers with a diameter of 0.6 mm and a length of 50 mm.

The structural characteristics of the Nd^{3+}- and Tm^{3+}-doped $YScO_3$ crystal fibers have been described in our earlier works [18,37,38]. The X-ray pattern of $YScO_3$ includes good narrow peaks, which points to a high degree of crystallinity. According to X-ray data, the $YScO_3$ crystal fiber is homogeneous and belongs to the bixbyite structural type (space group *Ia*3).

Time-resolved luminescence and excitation spectra and kinetics of luminescence decay of both Nd^{3+} and Tm^{3+} ions in $YScO_3$ crystal fiber were measured on the MDR-23 monochromator (LOMO, Saint-Petersburg, Russia) at temperatures of 77 and 300 K. The Solar LP-604 parametric generator (Solar LS, Minsk, Belarus) was used as a source of excitation. The luminescence excitation spectra were measured by scanning the irradiation of the Solar LP-604 tunable parametric generator across the absorption bands of both Nd^{3+} and Tm^{3+} ions while keeping the absorption intensity of the laser emission on the studied transitions constant ($\lambda_{det.}$ = const). The decay kinetics of luminescence was measured using the double selection method (based on luminescence spectrum and excitation). The luminescence from the studied samples was focused into the slit of the monochromator using a condenser, and the signal was subsequently detected using the FEU-83 and Hamamatsu R5108 photomultipliers (Hamamatsu Photonics, Sendai City, Japan) and a PbS photosensitive resistor. The signal from the detectors was fed into the Tektronix–TDS3052B wideband (0–500 MHz) oscilloscope (Tektronix, Beaverton, OR, USA) connected to a computer.

All measurements were carried out at temperatures of 77 and 300 K. The width of the spectral lines depends on the value of an electron—the phono interaction of the impurity center with the phonon field of the crystal lattice. In spectroscopy, this parameter is characterized by homogeneous broadening. At 77 K, phonons are frozen up to the energy of kT = 51 cm^{-1}, resulting in the narrowing of luminescence lines and a decrease in the value of homogeneous linewidth. At 300 K, phonons with energy up to kT = 210 cm^{-1} are involved, resulting in an increase in nonradiative relaxation channels, leading to broadening

of luminescence lines. This effect is especially pronounced for lines in the long-wavelength region of the luminescence spectrum where inter-Stark transitions of both Nd^{3+} and Tm^{3+} ion levels are involved in nonradiative relaxation processes.

3. Results and Discussion

3.1. Spectroscopy of Nd^{3+}:$YScO_3$

Normalized time-resolved luminescence excitation spectra of Nd^{3+} ions in the $YScO_3$ host were recorded at a temperature of 77 K, as shown in Figure 1. The spectra have been measured in the spectral range of 780–850 nm. Luminescence excitation spectra have been obtained through the scanning of parametric laser radiation on the $^4I_{9/2} \rightarrow {}^4F_{5/2} + {}^2H_{9/2}$ electron transitions and selective detection of luminescence on the $^4F_{3/2} \rightarrow {}^4I_{9/2}$ ($\lambda_{det.}$ = 896 nm). The luminescence excitation spectra are modified and intensities between spectral lines, in particular 821.4 and 823.8 nm, are redistributed with changes in delay times of 20 μs to 254 μs relative to the moment of laser excitation. Analysis of the changes in luminescence excitation spectra allows us to assume that two types of Nd^{3+} optical centers exist in the $YScO_3$ host.

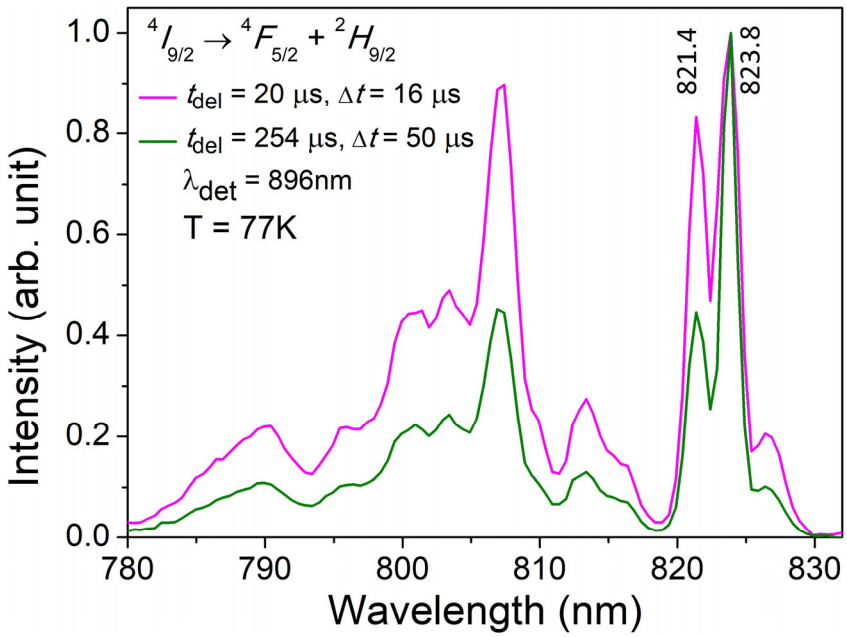


Figure 1. Low-temperature (77 K) time-resolved luminescence excitation spectra of Nd^{3+} ion in $YScO_3$ host being measured in the $^4I_{9/2} \rightarrow {}^4F_{5/2} + {}^2H_{9/2}$ electron transitions. A delay time and a gate used were $t_{del(1)}$ = 20 μs and $\Delta t_{(1)}$ = 16 μs, respectively; $t_{del(2)}$ = 254 μs and $\Delta t_{(2)}$ = 50 μs, respectively.

Time-resolved luminescence spectra of Nd^{3+} ion in the $YScO_3$ crystal fiber have been measured on the $^4F_{3/2} \rightarrow {}^4I_{9/2,11/2}$ electron transitions at 77 and 300 K. Nd^{3+} ions have been excited at 823.8 and 821.4 nm on the $^4I_{9/2} \rightarrow {}^4F_{5/2} + {}^2H_{9/2}$ electron transitions. Figure 2a,c show luminescence spectra of Nd^{3+} on the $^4F_{3/2} \rightarrow {}^4I_{9/2}$ electron transition being measured at excitation of 823.8 and 821.4 nm, respectively. Luminescence spectra of Nd^{3+} ions change with the excitation wavelength. Double selection for excitation wavelength and time leads to shifting luminescence lines. Double selection shows that luminescence spectra of Nd^{3+} ions change with the excitation wavelength and delay times relative to the moment of laser excitation. Analysis of luminescence spectra of Nd^{3+} ions allows us to determine the number of spectral lines being recorded at two different excitation wavelengths. In both cases, the spectra of Nd^{3+} on the $^4F_{3/2} \rightarrow {}^4I_{9/2}$ electron transition includes five Stark components (T = 77 K) that correspond to the number of lines $(2J + 1)/2$ being predicted by theory. This points to complete removal of degeneration of the electron transitions.

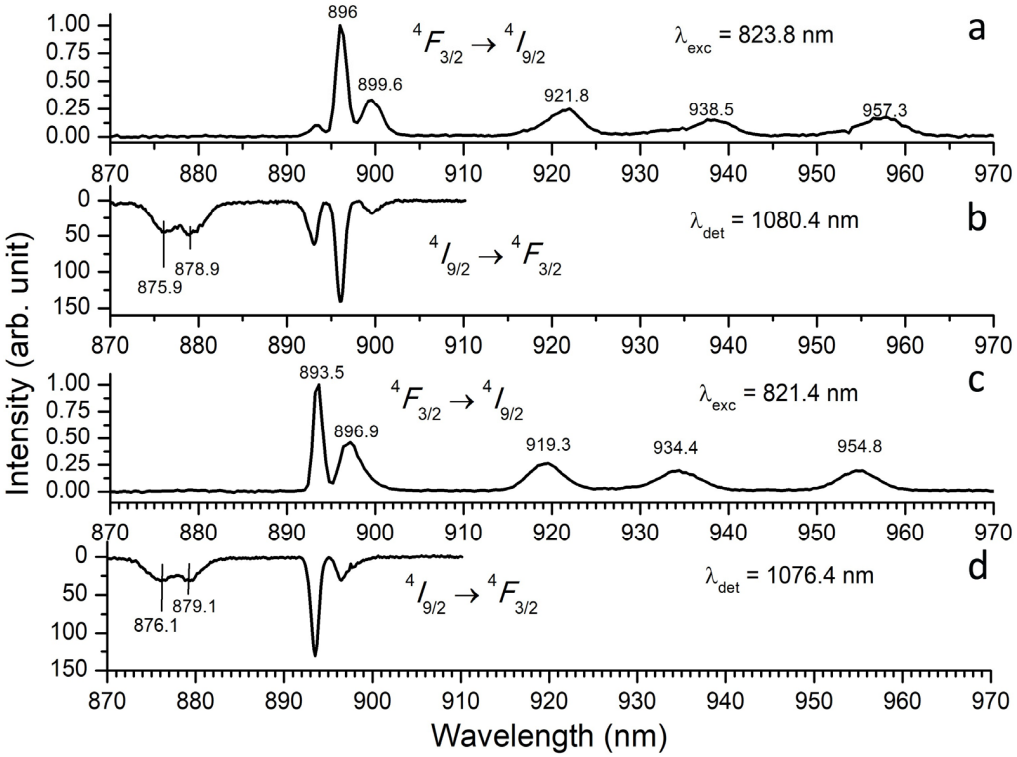


Figure 2. (**a**,**c**) Low-temperature time-resolved luminescence spectra of Nd^{3+} ions in $YScO_3$ being measured on the $^4F_{3/2} \rightarrow {}^4I_{9/2}$ electron transition at excitation of 823.8 nm (center I) and 821.4 nm (center II), respectively. (**b**,**d**) Luminescence excitation spectra of Nd^{3+} ions being measured on the $^4I_{9/2} \rightarrow {}^4F_{5/2} + {}^2H_{9/2}$ electron transitions at detection on 1080.4 nm (center I) and 1076.4 nm (center II), respectively. For all spectra, a delay time and a gate used were t_{del} = 10 μs and Δt = 6 μs, respectively.

So, the $^4I_{9/2}$ electron level splits into five components. $^4F_{3/2}$ and $^4I_{11/2}$ split into two and six Stark components, respectively, at each excitation wavelength. Spectral lines are shifting with excitation wavelength, but its number remains the same. This fact points to the presence of two types of Nd^{3+} optical centers. The number of Stark components and values of splitting allow us to conclude that both centers have low site symmetry of C_2.

Normalized luminescence spectra of Nd^{3+} ions in $YScO_3$ have been measured on the $^3F_{3/2} \rightarrow {}^4I_{11/2}$ electron transition at excitation of 823.8 and 821.4 nm and temperatures of 77 and 300 K (Figure 3a,b). Analysis of luminescence spectra of the $^3F_{3/2} \rightarrow {}^4I_{11/2}$ shows that the increase in time delay relative to the moment of laser excitation leads to a shift of spectral lines and redistribution of their intensities on the $^3F_{3/2} \rightarrow {}^4I_{9/2}$ electron transition. The changes in luminescence spectra allow us to identify spectral lines of Nd^{3+} ions and distinguish two group of lines and hence two types of Nd^{3+} optical centers in the $YScO_3$ host.

Figure 4a,b show luminescence decay kinetics of Nd^{3+}:YSO_3 being measured at excitation of 823.8 and 821.4 nm ($^4F_{9/2} \rightarrow {}^4F_{5/2} + {}^2H_{9/2}$ electron transition) and temperatures of 77 and 300 K. The LP-604 (Solar LS) parametric generator has been used as an excitation source. The luminescence kinetics have been recorded on the $^4F_{3/2} \rightarrow {}^4I_{9/2}$ electron transition. Approximation of luminescence decay curves of Nd^{3+}:$YScO_3$ being measured at excitation of λ_{exc} = 823.8 nm, detection of λ_{det} = 896.0 nm, and temperatures of 77 and 300 K shows that each of the decay curves is described by two exponential models, with lifetimes of τ_1(300 K) = 100/250 μs; τ_1(77 K) = 130/290 μs (Figure 4a). At excitation of λ_{exc} = 821.4 nm and detection of λ_{det} = 893.5 nm, luminescence decay curves consist of two exponents with lifetimes of τ_2(300 K) = 100/240 μs and τ_2(77 K) = 130/250 μs (Figure 4b).

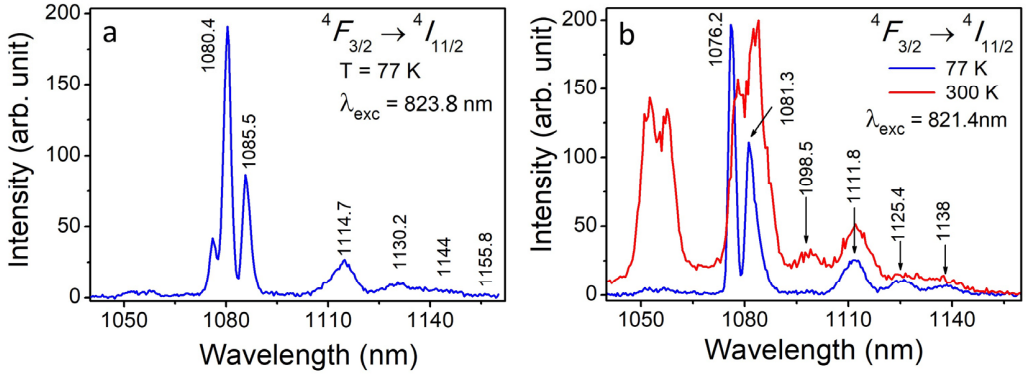


Figure 3. (**a**) Luminescence spectrum of Nd^{3+} ions in $YScO_3$ crystal fiber being measured on the $^4F_{3/2} \rightarrow {}^4I_{11/2}$ at an excitation of 823.8 nm ($^4I_{9/2} \rightarrow {}^4F_{5/2} + {}^2H_{9/2}$ electron transition, center I), a delay time of 10 μs, a gate of 6 μs, and a temperature of 77 K. (**b**) Luminescence spectra of Nd^{3+} ions in $YScO_3$ crystal fiber being measured on the $^4F_{3/2} \rightarrow {}^4I_{11/2}$ at excitation of 821.4 nm ($^4I_{9/2} \rightarrow {}^4F_{5/2} + {}^2H_{9/2}$ electron transition, center II), a delay time of 10 μs, a gate of 6 μs, and a temperature of 77 and 300 K.

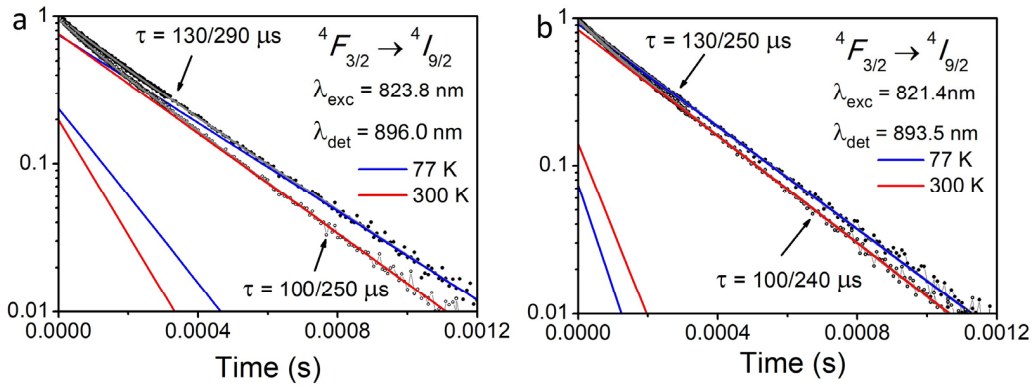


Figure 4. (**a**) Luminescence quenching kinetics of Nd $^{3+}$:YSO_3 being recorded at excitation of 823.8 nm ($^4I_{9/2} \rightarrow {}^4F_{5/2} + {}^2H_{9/2}$), detection wavelength of 896.0 nm ($^4F_{3/2} \rightarrow {}^4I_{11/2}$ electron transition), and temperatures of 77 and 300 K. (**b**) Luminescence quenching kinetics of Nd $^{3+}$:YSO_3 being recorded at excitation of 821.4 nm ($^4I_{9/2} \rightarrow {}^4F_{5/2} + {}^2H_{9/2}$), detection wavelength of 893.5 nm ($^4F_{3/2} \rightarrow {}^4I_{11/2}$ electron transition), and temperatures of 77 and 300 K.

Total intensity of luminescence decay kinetics of Nd^{3+}:$YScO_3$ is determined by the long-lifetime center (intensity ratio I_1/I_2 of 0.78/0.22, Figure 4a). The short-lifetime center is formed less effectively and its contribution to the total intensity is insignificant (intensity ratio I_1/I_2 of 0.94/0.06, Figure 4b). Figure 4a,b show that the lifetime of both centers is increasing with decreasing temperature down to 77 K. Decreasing temperature probably leads to decreasing electron–phonon interaction and intracenter nonradiative relaxation of the excitation energy.

The crystal structure of Nd^{3+}:$YScO_3$ has been described previously [18]. It was shown that neodymium ions can substitute basic ions of yttrium and scandium. The relation between ionic radii of yttrium (0.9 Å), scandium (0.83 Å), and neodymium (0.98 Å) is near the Goldschmidt criterion. Substitution of yttrium and scandium ions by neodymium does not require charge compensation in $YScO_3$. This leads to the formation of two basic types of optical center of Nd^{3+} activators with the local symmetry of C_2. However, a slight difference between cation radii leads to a local distortion in octahedra occupied by Nd^{3+}. The selective laser spectroscopy method is sensitive to these changes, and local distortion in the ion activator surrounding affects the spectral–kinetic characteristics of neodymium ion.

The third optical center with a short lifetime is probably the pair aggregate (Nd^{3+}–Nd^{3+}) one. The Nd^{3+}–Nd^{3+} center is formed in the neighboring MO_6 polyhedra sharing the O^{2-}–O^{2-} edge, where Nd^{3+} substitutes basic ions Y^{3+} and Sc^{3+}. The

multipole interaction of Nd^{3+} ions in the pair (Nd^{3+}–Nd^{3+}) leads to luminescence quenching and hence decreasing lifetime of the Nd^{3+} activator. The effect of this interaction depends on activator concentration as well as Nd^{3+}–Nd^{3+} distance. This is one of the reasons for the non-exponential character of kinetics at the beginning state of the luminescence quenching.

Spectral lines of the Nd^{3+} ion occupying the C_{3i} site are not observed because electro-dipole transitions are forbidden in rare-earth ions occupying centro-symmetric positions.

Analysis of luminescence excitation ($^4I_{9/2} \rightarrow {}^4F_{5/2} + {}^2H_{9/2}$ transitions) and luminescence spectra ($^4F_{3/2} \rightarrow {}^4I_{9/2}$, $^4I_{11/2}$ transitions) allows us to build the scheme of $^4I_{9/2}$,$^4I_{11/2}$, and $^4F_{3/2}$ Stark levels of Nd^{3+} ions, which occupy two positions with the site symmetry of C_2 in the $YScO_3$ crystal structure. Figure 5 shows the Stark energy for each of two basic Nd^{3+} optical centers with site symmetry of C_2. The first center C_2 (I) is formed in the result of substitution of Y^{3+} by Nd^{3+}, and the second center C_2 (II) is a result of the substitution of Sc^{3+} by Nd^{3+}.

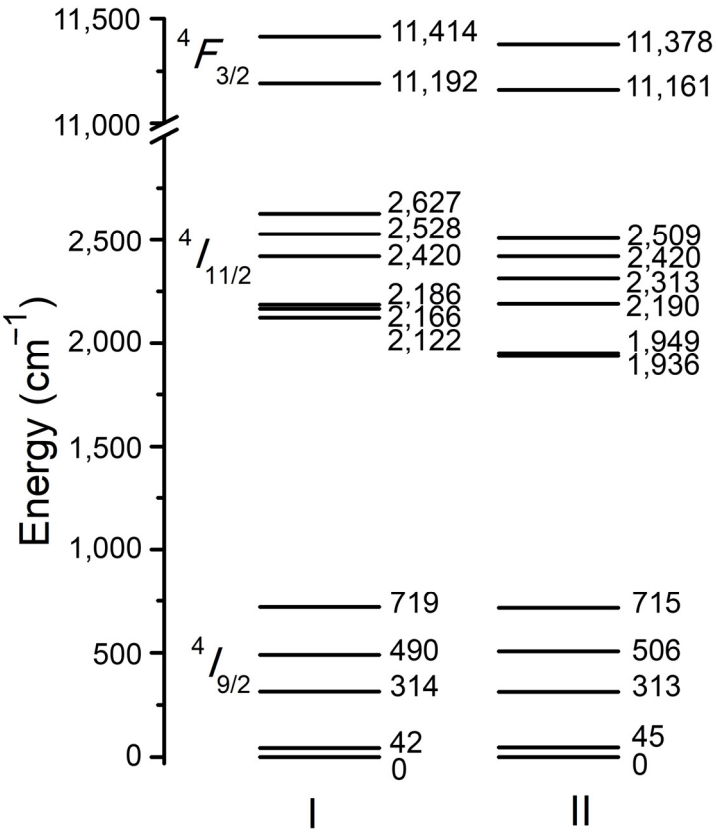


Figure 5. Scheme of $^4I_{9/2}$,$^4I_{11/2}$, and $^4F_{3/2}$ Stark levels for two types of Nd^{3+} centers with a site symmetry of C_2 (I) and C_2 (II) in $YScO_3$ crystal structure.

Both Nd^{3+} optical centers have a site symmetry of C_2 but depend on Nd–O distance in a structural polyhedra where Nd^{3+} substitutes Y^{3+} (center I) or Sc^{3+} (center II). Isomorphic substitution of basic structural cations (Y^{3+} and Sc^{3+}) by Nd^{3+} in a local position leads to changes in the crystal field around Nd^{3+} ions, but the type of local symmetry remains C_2. So, we can distinguish two different optical centers C_2 (I) and C_2 (II) with almost equal lifetimes and values of Stark splitting of $^4I_{9/2}$, $^4I_{11/2}$, and $^4F_{3/2}$ levels (Figures 4 and 5).

3.2. Spectroscopy of Tm^{3+}:$YScO_3$

Figure 6 shows low-temperature (T = 77 K) time-resolved luminescence excitation spectra of the 0.1 at. % Tm^{3+}:$YScO_3$ crystal fiber. The luminescence excitation spectra have been recorded at the LP-604 parametric laser radiation in the spectral range of 1160 to

1230 nm ($^3H_6 \rightarrow {}^3H_5$ transition) and registration of luminescence at 1945.6 nm ($^3F_4 \rightarrow {}^3H_6$ transition).

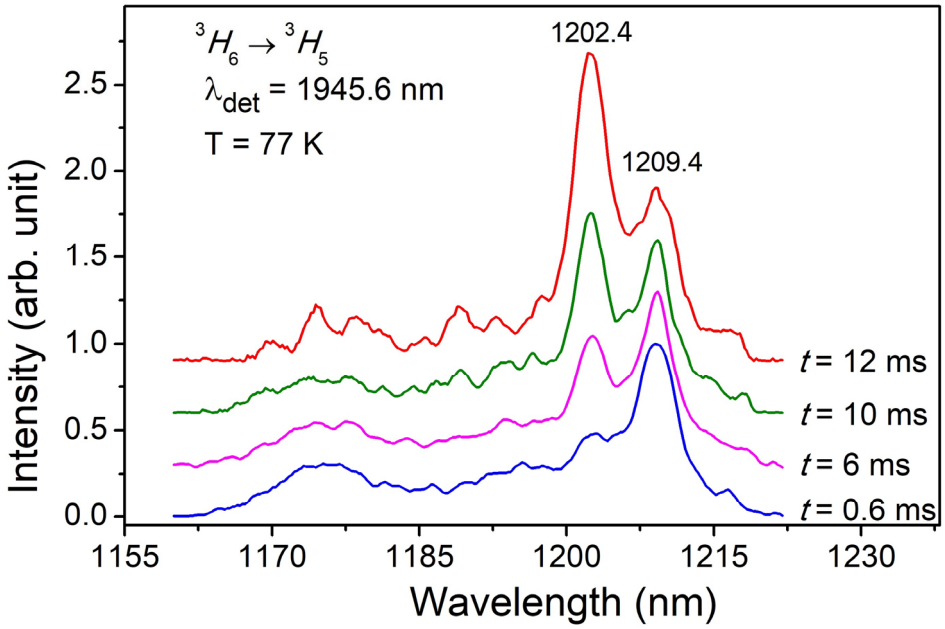


Figure 6. Normalized time-resolved luminescence excitation spectra of Tm^{3+}:$YScO_3$ being measured on the $^3H_6 \rightarrow {}^3H_5$ transition at 77 K. Registration wavelength was 1945.6 nm. Delay times used were 0.6 ms, 6 ms, 10 ms and 12 ms.

Changes in time delay of 0.6 ms to 12 ms relative to the moment of laser excitation lead to changes in luminescence excitation spectra, intensity redistribution between spectral lines of 1202.4 and 1209.4 nm. Changes being observed in luminescence excitation spectra allow us to assume that two types of optical centers of Tm^{3+} ions exist in the $YScO_3$ crystal structure.

The luminescence of Tm^{3+}:$YScO_3$ has been measured on the $^3F_4 \rightarrow {}^3H_6$ electron transition (spectral range of 1600–2240 nm) at selective laser excitation of 1202.4 and 1209.4 nm ($^3H_6 \rightarrow {}^3H_5$ electron transition). Figure 7a,c show time-resolved luminescence spectra of Tm^{3+}:YSO_3 being measured at temperatures of 77 and 300 K and laser excitation of 1202.35 nm. The luminescence spectra of Tm^{3+} ions show slight changes in spectral line profile. The luminescence line intensities are redistributing, depending on the time delay relative to the moment of laser excitation (0.6 to 12 ms). However, the Stark structure is poorly resolved. The low-temperature (77 K) luminescence spectra being measured on the $^3F_4 \rightarrow {}^3H_6$ electron transition are non-structured (Figure 7c), as are the room-temperature (300 K) ones. To identify and assign the luminescence lines to specific optical centers has become a difficult task. First, the luminescence spectra of the Tm^{3+} ion include many Stark components of $^3F_4$ (9 ones) and $^3H_6$ (13 ones), and the mean values of Stark splitting are sufficiently low. Second, the spectral lines of the Tm^{3+} ion are broadened and overlapped due to high values of electron–phonon interaction.

Figure 7b,d show luminescence quenching kinetics of Tm^{3+}:$YScO_3$ being measured at excitation of 1202.4 nm ($^3H_6 \rightarrow {}^3H_5$ electron transition) and registration on 1944 nm in the $^3F_4 \rightarrow {}^3H_6$ electron transition at temperatures of 300 and 77 K. Each luminescence quenching curve is described by two exponential models with lifetimes of τ (300 K) = 3.8/17 ms (I_1/I_2 = 0.96/0.04) and τ (77 K) = 4.25/19 ms (I_1/I_2 = 0.9/0.1). Short-time exponents (τ (300 K) = 3.8 and τ (77 K) = 4.25 ms) make a major contribution to luminescence quenching kinetics of the Tm^{3+} ion. Decreasing temperature down to 77 K leads to increasing the lifetime of the Tm^{3+} ion up to 11%. The contribution of the long-time component in the total intensity of luminescence quenching kinetics is low.

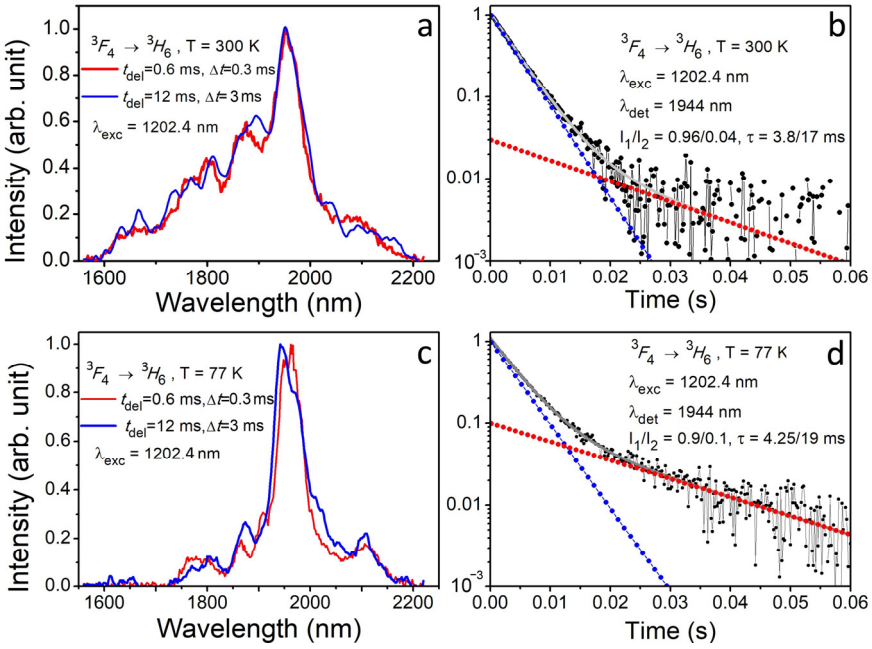


Figure 7. (**a**) Time-resolved luminescence spectra of Tm^{3+}:$YScO_3$ crystal fiber being measured on the $^3F_4 \rightarrow {}^3H_6$ electron transition at excitation of 1202.4 nm ($^3H_6 \rightarrow {}^3H_5$ electron transition) and a temperature of 300 K. (**b**) Luminescence quenching kinetics of Tm^{3+}:$YScO_3$ being measured at excitation of 1202.4 nm and detection wavelengths of 1944 nm at 300 K. (**c**) Low-temperature (77 K) time-resolved luminescence spectra of Tm^{3+}:$YScO_3$ being measured at excitation of 1202.4 nm ($^3H_6 \rightarrow {}^3H_5$ electron transition). (**d**) Luminescence quenching kinetics of Tm^{3+}:$YScO_3$ being measured on the $^3F_4 \rightarrow {}^3H_6$ electron transition at excitation of 1202.4 nm and detection wavelengths of 1944 nm at 77 K. For all spectra, a delay time and a gate used were $t_{del(1)}$ = 0.6 ms and $\Delta t_{(1)}$ = 0.3 ms, respectively; $t_{del(2)}$ = 12 ms and $\Delta t_{(2)}$ = 3 ms, respectively.

Figure 8a,c show normalized time-resolved luminescence spectra of Tm^{3+}:$YScO_3$ being measured at excitation of 1209.4 nm ($^3H_6 \rightarrow {}^3H_5$ electron transition) and temperatures of 77 and 300 K. The luminescence spectra are modified, and the line intensities are redistributed with time delay. Decreasing the temperature down to 77 K does not improve structurization of luminescence spectra in the $^3F_4 \rightarrow {}^3H_6$ electron transition in the Tm^{3+} ion (Figure 8c). Due to the poorly resolved Stark structure, identifying and assigning lines to specific centers is difficult. This is the result of the high value of electron–phonon interaction, overlapping spectral lines, and low values of splitting of $^3F_4$ and $^3H_6$ Stark levels.

Figure 8b,d show luminescence quenching kinetics in Tm^{3+}:$YScO_3$ at excitation of 1209.4 nm ($^3H_6 \rightarrow {}^3H_5$ electron transition) and registration of luminescence at 1944 nm ($^3F_4 \rightarrow {}^3H_6$ electron transition) at temperatures of 77 and 300 K. The luminescence quenching curves are described by a single exponent law with lifetimes of τ (300 K) = 3.2 and τ (77 K) = 3.7 ms at temperatures of 300 and 77 K, respectively. The difference in lifetime can be explained by the decrease in the intercenteral relaxation with temperature (down to 77 K).

Analysis of luminescence quenching kinetics of Tm^{3+}:$YScO_3$ (Figures 7b,d and 8b,d) shows three types of Tm^{3+} optical centers in the crystal structure. Two of them are basic with short lifetimes of τ_1 (300 K) = 3.2 ms, τ_1 (77 K) = 3.7 ms and τ_2 (300 K) = 3.8 ms, τ_2 (77 K) = 4.25 ms. These centers belong to the low local symmetry of C_2. One of them is formed as the result of the local substitution of Y^{3+} by Tm^{3+} and another one is due to the local substitution of Sc^{3+} by Tm^{3+}. The third one has a local site of C_{3i} and lifetimes of τ_3 (300 K) = 17 ms (I = 0.04) and τ_3 (77 K) = 19 ms (I = 0.1) at 300 and 77 K, respectively. The third center has longer lifetime and higher local symmetry (C_{3i}).

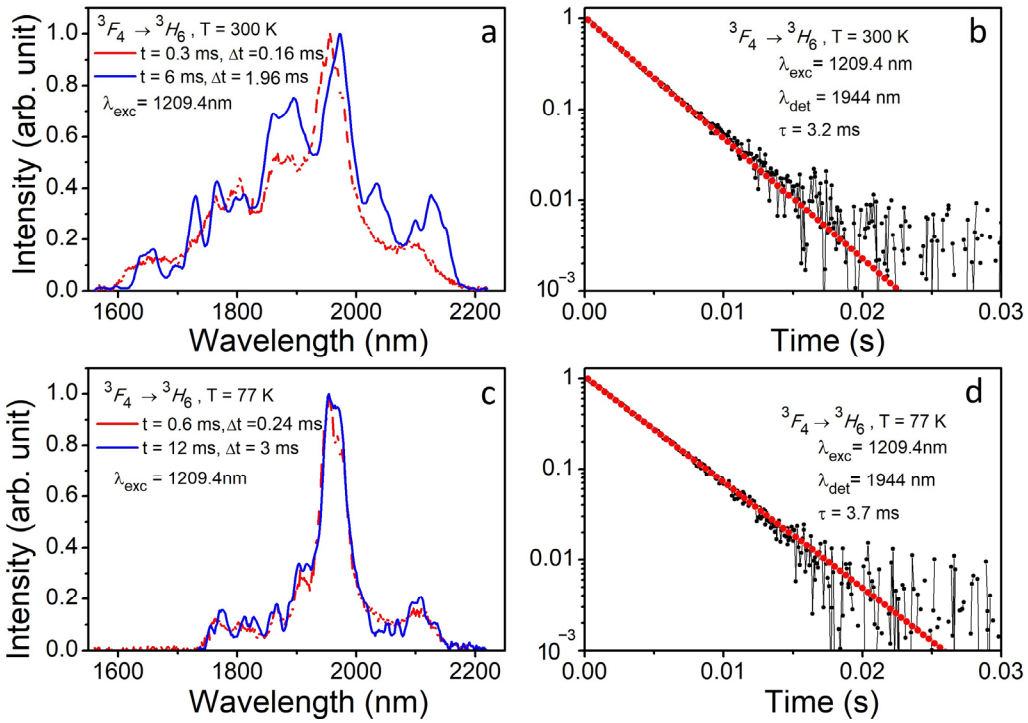


Figure 8. (**a**) Time-resolved luminescence spectra of Tm^{3+}:$YScO_3$ ion ($^3F_4 \rightarrow {}^3H_6$ electron transition) being measured at an excitation of 1209.4 nm ($^3H_6 \rightarrow {}^3H_5$ electron transition) at a temperature of 300 K. A delay time and a gate used were $t_{del(1)}$ = 0.3 ms and $\Delta t_{(1)}$ = 0.16 ms, respectively; $t_{del(2)}$ = 6 ms and $\Delta t_{(2)}$ = 1.96 ms, respectively. (**b**) Luminescence quenching kinetics of Tm^{3+} ion being measured at an excitation of 1209.4 nm and detection wavelengths of 1944 nm. (**c**) Time-resolved luminescence spectra of Tm^{3+}:$YScO_3$ being measured on the $^3H_6 \rightarrow {}^3H_5$ electron transition at an excitation of 1209.4 nm and a temperature of 77 K. A delay time and a gate used were $t_{del(1)}$ = 0.6 ms and $\Delta t_{(1)}$ = 0.24 ms, respectively; $t_{del(2)}$ = 12 ms and $\Delta t_{(2)}$ = 3 ms, respectively. (**d**) Luminescence quenching kinetics of Tm^{3+}:$YScO_3$ being measured on the $^3F_4 \rightarrow {}^3H_6$ electron transition at an excitation of 1209.4 nm and a detection of 1944 nm at 77 K.

4. Conclusions

The substitution of Y^{3+} and Sc^{3+} by Nd^{3+} ions in the crystal structure of the $YScO_3$ crystal fiber leads to the formation of three types of Nd^{3+} optical centers. Two of these dominate and exhibit a local symmetry of C_2. The lifetimes of the Nd^{3+} optical centers in the $YScO_3$ crystal fiber were determined at two different temperatures. For the center I, the lifetimes were measured to be τ_1(300 K) = 250 μs and τ_1(77 K) = 290 μs. For the center II, the lifetimes were determined to be τ_2(300 K) = 240 μs and τ_2(77 K) = 250 μs. In addition to the two dominant optical centers, a third optical center with shorter lifetimes has been observed in the YScO3 crystal fiber. The third center, likely a Nd^{3+}–Nd^{3+} aggregate pair, exhibits lifetimes of τ_3(300 K) = 100 μs and τ_3(77 K) = 130 μs. This aggregate pair is believed to form as a result of the local substitution of Nd^{3+} for the basic structural cation (Y^{3+} and Sc^{3+}) in the neighboring octahedra that share an edge. The quenching of Nd^{3+} luminescence is primarily ascribed to a combination of interaction between neighboring Nd^{3+} ions and the process of nonradiative relaxation of the excitation energy. The Stark component scheme for $^4F_{3/2}$, $^4I_{11/2}$, and $^4I_{9/2}$ electron levels in the Nd^{3+} ion has been built for both basic optical centers with the local symmetry of C_2.

Two short-lifetime optical centers of Tm^{3+} ions with the local symmetry of C_2 are formed in the $YScO_3$ crystal fiber through the substitution of Y^{3+} and Sc^{3+} with Tm^{3+} ions. The lifetimes of these optical centers have been estimated as τ_1 (300 K) = 3.8 ms and τ_1(77 K) = 4.25 ms for center I, and τ_2 (300 K) = 3.2 ms and τ_2 (77 K) = 3.7 ms for center II.

The third center with long lifetimes of τ_3 (300 K) = 17 ms and τ_3 (77 K) = 19 ms has a local symmetry classified as C_{3i}.

Author Contributions: Conceptualization, V.T. and E.D.; methodology, O.A. and S.R.; validation, O.A. and E.D.; formal analysis, O.A. and E.D.; investigation, O.A. and E.D.; resources, V.K.; data curation, O.A. and E.D.; writing—original draft preparation, E.D. and O.A.; writing—review and editing, E.D., O.A. and V.T.; visualization, E.D. and O.A.; supervision, E.D. and V.T.; funding acquisition, E.D. and V.T. All authors have read and agreed to the published version of the manuscript.

Funding: This research was funded by the Russian Science Foundation, grant number 22-22-00968.

Institutional Review Board Statement: Not applicable.

Informed Consent Statement: Not applicable.

Data Availability Statement: Data sharing is not applicable for this article.

Conflicts of Interest: The authors declare no conflict of interest.

References

1. Klein, P.H.; Croft, W.J. Thermal Conductivity, Diffusivity, and Expansion of Y_2O_3, $Y_3Al_5O_{12}$, and LaF_3 in the Range 77°–300° K. *J. Appl. Phys.* **1967**, *38*, 1603. [CrossRef]
2. Nigara, Y. Measurement of the Optical Constants of Yttrium Oxide. *Jpn. J. Appl. Phys.* **1968**, *7*, 404. [CrossRef]
3. Petermann, K. Oxide Laser Crystals Doped with Rare Earth and Transition Metal Ions. In *Handbook of Solid-State Lasers: Materials, Systems and Applications*; Elsevier: Amsterdam, The Netherlands, 2013; pp. 3–27.
4. Fornasiero, L.; Mix, E.; Peters, V.; Petermann, K.; Huber, G. New Oxide Crystals for Solid State Lasers. *Cryst. Res. Technol.* **1999**, *34*, 255–260. [CrossRef]
5. Zhou, Z.; Guan, X.; Huang, X.; Xu, B.; Xu, H.; Cai, Z.; Xu, X.; Liu, P.; Li, D.; Zhang, J.; et al. Tm^{3+}-Doped $LuYO_3$ Mixed Sesquioxide Ceramic Laser: Effective 205 Mm Source Operating in Continuous-Wave and Passive Q-Switching Regimes. *Opt. Lett.* **2017**, *42*, 3781. [CrossRef]
6. Liu, W.; Lu, D.; Guo, R.; Wu, K.; Pan, S.; Hang, Y.; Sun, D.; Yu, H.; Zhang, H.; Wang, J. Broadening of the Fluorescence Spectra of Sesquioxide Crystals for Ultrafast Lasers. *Cryst. Growth Des.* **2020**, *20*, 4678–4685. [CrossRef]
7. Moncorgé, R.; Guyot, Y.; Kränkel, C.; Lebbou, K.; Yoshikawa, A. Mid-Infrared Emission Properties of the Tm3+-Doped Sesquioxide Crystals Y_2O_3, Lu_2O_3, Sc_2O_3 and Mixed Compounds $(Y,Lu,Sc)_2O_3$ around 1.5-, 2- and 2.3-Mm. *J. Lumin.* **2022**, *241*, 118537. [CrossRef]
8. Li, S.; Zhang, L.; Tan, X.; Deng, W.; He, M.; Chen, G.; Xu, M.; Yang, Y.; Zhang, S.; Zhang, P.; et al. Growth, Structure, and Spectroscopic Properties of a Tm^{3+}, Ho^{3+} Co-Doped Lu_2O_3 Crystal for ~2.1 Mm Lasers. *Opt. Mater.* **2019**, *96*, 109277. [CrossRef]
9. Antoinette, M.M.; Israel, S.; Berchmans, J.L.; Manoj, G.J. Enhanced Photoluminescence and Charge Density Studies of Novel $(Sm_{1-x}Gd_x)_2O_3$ Nanophosphors for WLED Applications. *J. Mater. Sci. Mater. Electron.* **2018**, *29*, 19368–19381. [CrossRef]
10. Reenabati Devi, K.; Dorendrajit Singh, S.; David Singh, T. Photoluminescence Properties of White Light Emitting La_2O_3:Dy^{3+} Nanocrystals. *Indian J. Phys.* **2018**, *92*, 725–730. [CrossRef]
11. Antoinette, M.M.; Israel, S.; Amali, A.J.; Berchmans, J.L.; Kumar, B.S.; Manoj, G.J.; Usmaniya, U.M. A Novel Synthesis of Orange-Red Emitting $(Sm_{1-x}Ce_x)_2O_3$ Nanophosphors for UV LEDs. *Nano-Struct. Nano-Objects* **2018**, *13*, 51–58. [CrossRef]
12. Barrera, E.W.; Cascales, C.; Pujol, M.C.; Park, K.H.; Choi, S.B.; Rotermund, F.; Carvajal, J.J.; Mateos, X.; Aguiló, M.; Díaz, F. Synthesis of Tm:Lu_2O_3 Nanocrystals for Phosphor Blue Applications. *Phys. Proced.* **2010**, *8*, 142–150. [CrossRef]
13. Kumar, A.; Tiwari, S.P.; Kumar, K.; Rai, V.K. Structural and Optical Properties of Thermal Decomposition Assisted Gd_2O_3:Ho^{3+}/Yb^{3+} Upconversion Phosphor Annealed at Different Temperatures. *Spectrochim. Acta A Mol. Biomol. Spectrosc.* **2016**, *167*, 134–141. [CrossRef] [PubMed]
14. Tseng, K.P.; Yang, Q.; McCormack, S.J.; Kriven, W.M. High-Entropy, Phase-Constrained, Lanthanide Sesquioxide. *J. Am. Ceram. Soc.* **2020**, *103*, 569–576. [CrossRef]
15. El-Kelany, K.E.; Ravoux, C.; Desmarais, J.K.; Cortona, P.; Pan, Y.; Tse, J.S.; Erba, A. Spin Localization, Magnetic Ordering, and Electronic Properties of Strongly Correlated Ln_2O_3 Sesquioxides (Ln = La, Ce, Pr, Nd). *Phys. Rev. B* **2018**, *97*, 245118. [CrossRef]
16. Balabanov, S.; Demidova, K.; Filofeev, S.; Ivanov, M.; Kuznetsov, D.; Li, J.; Permin, D.; Rostokina, E. Influence of Lanthanum Concentration on Microstructure of $(Ho_{1-X}La_x)_2O_3$ Magneto-Optical Ceramics. *Phys. Status Solidi B Basic. Res.* **2020**, *257*, 1900500. [CrossRef]
17. Balabanov, S.S.; Filofeev, S.V.; Ivanov, M.G.; Kalinina, E.G.; Kuznetsov, D.K.; Permin, D.A.; Rostokina, E.Y. Self-Propagating High-Temperature Synthesis of $(Ho_{1-X}La_x)_2O_3$ Nanopowders for Magneto-Optical Ceramics. *Heliyon* **2019**, *5*, e01519. [CrossRef]
18. Alimov, O.; Dobretsova, E.; Guryev, D.; Kashin, V.; Kiriukhina, G.; Kutovoi, S.; Rusanov, S.; Simonov, S.; Tsvetkov, V.; Vlasov, V.; et al. Growth and Characterization of Neodymium-Doped Yttrium Scandate Crystal Fiber with a Bixbyite-Type Crystal Structure. *Cryst. Growth Des.* **2020**, *20*, 4593–4599. [CrossRef]

19. Pauling, L.; Shappell, M.D. The Crystal Structure of Bixbyite and the C-Modification of the Sesquioxides. *Z. Krist. Cryst. Mater.* **1930**, *75*, 128–142. [CrossRef]
20. Clark, J.B.; Richter, P.W.; Toit, L. du High-Pressure Synthesis of $YScO_3$, $HoScO_3$, $ErScO_3$, and $TmScO_3$, and a Reevaluation of the Lattice Constants of the Rare Earth Scandates. *J. Solid. State Chem.* **1978**, *23*, 129–134. [CrossRef]
21. Hanic, F.; Hartmanová, M.; Knab, G.G.; Urusovskaya, A.A.; Bagdasarov, K.S. Real Structure of Undoped Y_2O_3 Single Crystals. *Acta Crystallogr. Sect. B* **1984**, *40*, 76–82. [CrossRef]
22. Geller, S.; Romo, P.; Remeika, J.P. Refinement of the Structure of Scandium Sesquioxide. *Z. Fur Krist.—New Cryst. Struct.* **1967**, *124*, 136–142. [CrossRef]
23. Moore, P.B.; Araki, T. Braunite: Its Structure and Relationship Insights on the Genealogy of to Bixbyite, and Some Fluorite Derivative Structures. *Am. Mineral.* **1976**, *61*, 1226–1240.
24. Kitazawa, K.; Fueki, K. Effect of Point Defects on Laser Oscillation Properties of Nd-Doped Y_2O_3. *Jpn. J. Appl. Phys.* **1982**, *21*, 1017. [CrossRef]
25. Stone, J.; Burrus, C.A. Nd:Y_2O_3 Single-Crystal Fiber Laser: Room-Temperature Cw Operation at 1.07- and 1.35-Mm Wavelength. *J. Appl. Phys.* **1978**, *49*, 2281. [CrossRef]
26. Chang, N.C.; Gruber, J.B.; Leavitt, R.P.; Morrison, C.A. Optical Spectra, Energy Levels, and Crystal-Field Analysis of Tripositive Rare Earth Ions in Y_2O_3. I. Kramers Ions in C_2 Sites. *J. Chem. Phys.* **1982**, *76*, 3877–3889. [CrossRef]
27. Leavitt, R.P.; Gruber, J.B.; Chang, N.C.; Morrison, C.A. Optical Spectra, Energy Levels, and Crystal-Field Analysis of Tripositive Rare-Earth Ions in Y_2O_3. II. Non-Kramers Ions in C_2 Sites. *J. Chem. Phys.* **1982**, *76*, 4775–4788. [CrossRef]
28. Morrison, C.A.; Leavitt, R.P.; Gruber, J.B.; Chang, N.C. Optical Spectra, Energy Levels, and Crystal-Field Analysis of Tripositive Rare-Earth Ions in Y_2O_3. III. Intensities and g Values for C_2 Sites. *J. Chem. Phys.* **1983**, *79*, 4758–4763. [CrossRef]
29. Gruber, J.B.; Leavitt, R.P.; Morrison, C.A.; Chang, N.C. Optical Spectra, Energy Levels, and Crystal-Field Analysis of Tripositive Rare-Earth Ions in Y_2O_3. IV. *C3i Sites. J. Chem. Phys.* **1985**, *82*, 5373–5378. [CrossRef]
30. Gruber, J.B.; Krupke, W.F.; Poindexter, J.M. Crystal-Field Splitting of Trivalent Thulium and Erbium J Levels in Yttrium Oxide. *J. Chem. Phys.* **1964**, *41*, 3363. [CrossRef]
31. Mandel, M. Paramagnetic Resonance of Yb^{3+} in Yttrium Oxide. *Appl. Phys. Lett.* **1963**, *2*, 197. [CrossRef]
32. Fornasiero, L.; Berner, N.; Dicks, B.-M.; Mix, E.; Peters, V.; Petermann, K.; Huber, G. Broadly Tunable Laser Emission from Tm:Y_2O_3 and Tm:Sc_2O_3 at 2 μm. In Proceedings of the Advanced Solid State Lasers, Boston, MA, USA, 31 January–3 February 1999; p. WD5.
33. Fornasiero, L.; Mix, E.; Peters, V.; Heumann, E.; Petermann, K.; Huber, G. Efficient Laser Operation of Nd:Sc_2O_3 at 966 nm, 1082 nm and 1486 nm. In Proceedings of the Advanced Solid State Lasers, Boston, MA, USA, 31 January–3 February 1999; p. MC6.
34. Liu, W.; Lu, D.; Pan, S.; Xu, M.; Hang, Y.; Yu, H.; Zhang, H.; Wang, J. Ligand Engineering for Broadening Infrared Luminescence of Kramers Ytterbium Ions in Disordered Sesquioxides. *Cryst. Growth Des.* **2019**, *19*, 3704–3713. [CrossRef]
35. Kränkel, C.; Uvarova, A.; Guguschev, C.; Kalusniak, S.; Hülshoff, L.; Tanaka, H.; Klimm, D. Rare-Earth Doped Mixed Sesquioxides for Ultrafast Lasers [Invited]. *Opt. Mater. Express* **2022**, *12*, 1074–1091. [CrossRef]
36. Reichert, F.; Fechner, M.; Koopmann, P.; Brandt, C.; Petermann, K.; Huber, G. Spectroscopy and Laser Operation of Nd-Doped Mixed Sesquioxides $(Lu_{1-x}Sc_x)_2O_3$. *Appl. Phys. B* **2012**, *108*, 475–478. [CrossRef]
37. Dobretsova, E.A.; Alimov, O.K.; Rusanov, S.Y.a.; Kashin, V.V.; Voronov, V.V.; Guryev, D.A.; Kutovoi, S.A.; Vlasov, V.I.; Tsvetkov, V.B. Spectroscopy of the Yttrium Scandate Doped by Thulium Ions. *Phys. Solid State* **2022**, *64*, 2238. [CrossRef]
38. Dobretsova, E.; Alimov, O.; Guryev, D.; Voronov, V.; Rusanov, S.; Kashin, V.; Kutovoy, S.; Vlasov, V.; Badyanova, L.; Novikov, I.; et al. Structural and Spectroscopic Features of the Bixbyite-Type Yttrium Scandate Doped by Rare-Earth Ions. *Crystals* **2022**, *12*, 1745. [CrossRef]
39. Feigelson, R.S. Pulling Optical Fibers. *J. Cryst. Growth* **1986**, *79*, 669–680. [CrossRef]
40. Bufetova, G.A.; Kashin, V.V.; Nikolaev, D.A.; Rusanov, S.Y.; Seregin, V.F.; Tsvetkov, V.B.; Shcherbakov, I.A.; Yakovlev, A.A. Neodymium-Doped Graded-Index Single-Crystal Fibre Lasers. *Quantum Elec.* **2006**, *36*, 616. [CrossRef]

Disclaimer/Publisher's Note: The statements, opinions and data contained in all publications are solely those of the individual author(s) and contributor(s) and not of MDPI and/or the editor(s). MDPI and/or the editor(s) disclaim responsibility for any injury to people or property resulting from any ideas, methods, instructions or products referred to in the content.